# Multi-segment coherent beam combining*

D. R. Neal, 1128
S. D. Tucker, 2338
R. Morgan, 1128
T. G. Smith, 2338
M. E. Warren, 1312
J. K. Gruetzner, 1128
R. R. Rosenthal, 2334
A. E. Bentley, 2338

Sandia National Laboratories, Department 1128
P. O. Box 5800, Albuquerque, NM 87185

## ABSTRACT

Scaling laser systems to large sizes for power beaming and other applications can sometimes be simplified by combining a number of smaller lasers. However, to fully utilize this scaling, coherent beam combination is necessary. This requires measuring and controlling each beam's pointing and phase relative to adjacent beams using an adaptive optical system.

We have built a sub-scale brass-board to evaluate various methods for beam-combining. It includes a segmented adaptive optic and several different specialized wavefront sensors that are fabricated using diffractive optics methods. We have evaluated a number of different phasing algorithms, including hierarchical and matrix methods, and have demonstrated phasing of several elements. The system is currently extended to a large number of segments to evaluate various scaling methodologies.

**Keywords:** adaptive optic, wavefront sensor, coherent beam combining

## 1. INTRODUCTION

There are a number of applications for high energy lasers, including power beaming[1], laser-driven wind tunnels[2], material processing[3], orbital debris removal[4], long range imaging[5], missile defense[6] and others. These systems, while very diverse in actual implementation, have in common the need for beams that have multiple megawatts of laser power, simultaneous with a coherent beam for long distance propagation. In fact, it is the extremely long range of several of these applications that drives the need for high energy. There have been several proposals for scaling lasers to high energy[7,8], and some key experimental demonstrations[9]. To date, chemical laser systems are the only demonstrated lasers with greater then 2 MW CW operation[10,11], although a number of proposed systems appear to be scaleable, given the appropriate investment (nuclear-pumped, free-electron, diode-laser). However, it is often during the scaling process that the fundamental problems with a given system come to light.

An alternative method for scaling lasers is to build many smaller lasers and then combine the individual beams coherently. There are a number of resonator schemes that can be used to couple numerous gain regions and produce multiple outputs that operate at the same frequency[12]. Unfortunately these systems all produce a number of separate, individual beams. To be useful for the long distance transmission applications, these individual beams must be combined together coherently. This involves more than just pointing them all in the same direction and removing dead space between. They must be phased together coherently.

The phasing problem is similar in many ways to the problems in segmented adaptive optics used for astronomy[13], and many of the techniques can be borrowed from this area of expertise. However, there are slightly different requirements: since all of the light originates from a single master (or distributed output) oscillator, the light can be single frequency. This reduces the requirements on the phasing systems, since absolute matching of path lengths is not required. Individual beams must have paths matched only to modulo $2\pi$ in phase. The other key difference is that many adaptive optics systems assume that the phase is continuous over the aperture. Thus individual slope measurements over a series of sub-apertures can be used to reconstruct the wavefront error. For a multiple beam

* This work was supported by the United States Department of Energy under contract number DE-AC04-94L85000.


0-8194-1893-5/95/$6.00

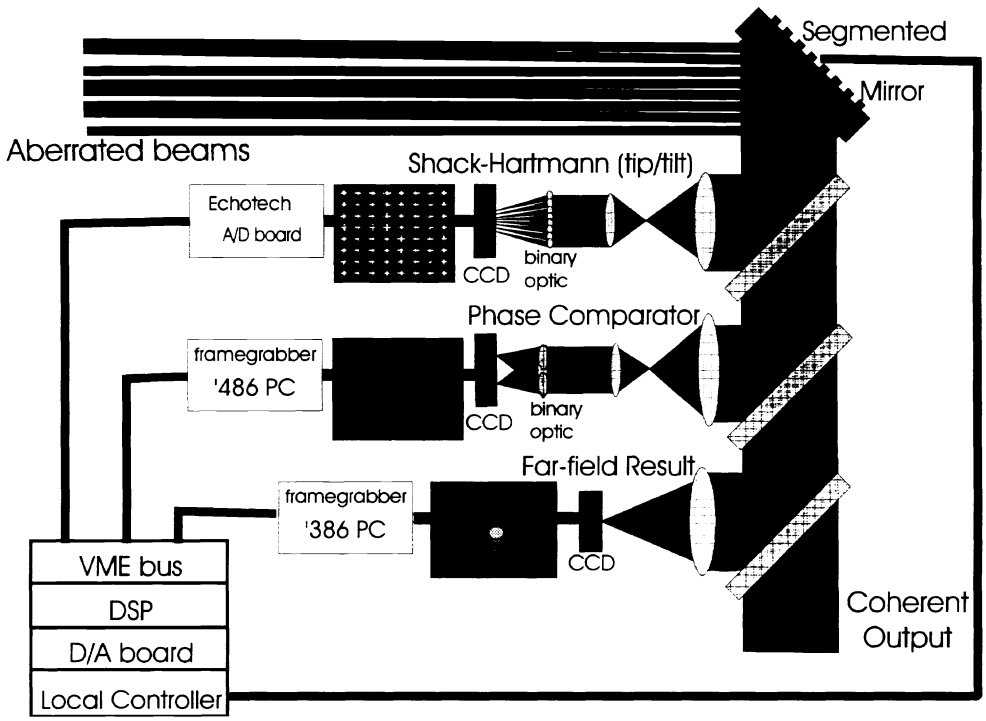


**Figure 1 - System diagram of beam combining testbed. There are three separate sensor systems, a Shack-Hartmann sensor for measuring tip/tilt of each segment, a phase comparator system for determining the overall piston phase, and a far-field sensor for performance evaluation.**

combining system, this is no longer true. Each beam can have its own relative phase. To construct the required wavefront, each beam must have its phase individually measured and compared to the adjacent beams and the whole.

Some of the systems require a very large number of beams. NASA has a power beaming program where they wish to use a 12 m diameter beam expander to combine as many as 144,000 individual beams[14]. The Sandia nuclear-pumped laser system would have approximately 512 separate channels, which may in turn be further subdivided[15]. A diode laser system would have millions of separate lasers. Thus the beam combining system must be able to combine coherently an extremely large number of beams. TTC has demonstrated astronomical applications of >1500 degrees of freedom (DOF) systems using segmented optics[16]. They used a shear plate system to measure the tip/tilt and piston of each segment and provide the required correction using a large DOF segmented adaptive optic. While this system is scaleable to some degree, the wavefront sensor is complicated and requires the integration of a large number of discrete optics and high sensitivity CCD cameras.

In previous work, we proposed the use of far field wavefront sensors and a hierarchical structure for scaling to large number of segments[17]. An optimizing controller was demonstrated on a six DOF system[18]. Others have used neural nets to phase more degrees of freedom simultaneously.[19] This work was extended to include the use of binary optics to allow for simple implementation of the hierarchical structure[20].

Unfortunately, the far-field wavefront sensing, while desirable from the point of view of simplicity, suffers from inherent ambiguities that make algorithmic phase determination difficult[21]. While it has some advantages over other techniques in its optical simplicity and the use of focused beams, it is operationally inefficient, requiring iterative solution techniques that aren't guaranteed to converge.

In this work we have extended the use$\xi$ of binary optics to the general beam combining problem. We have devised ways to compare beams segment by segment, while still preserving the hierarchical structure needed for scalability. The resulting systems are conceptually very simple and are easy to implement. The body of this paper will describe a brassboard testbed that is used to demonstrate the applications of binary optics to this problem.

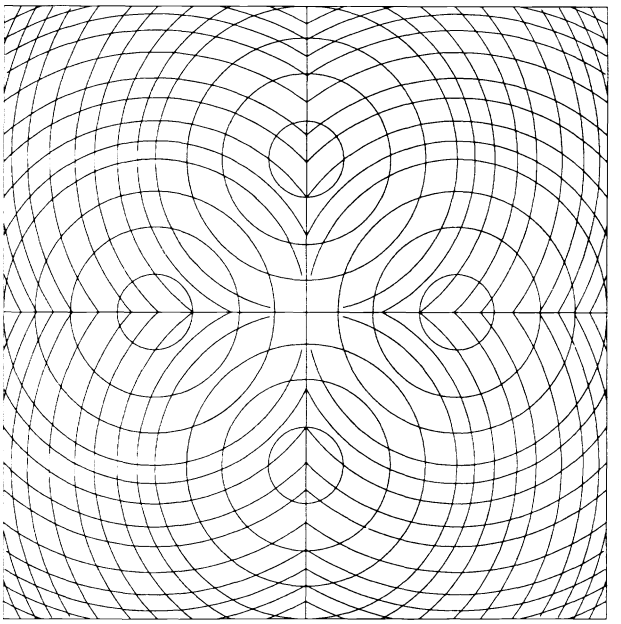

**Figure 2 - Overlapping lens elements are used to compare the phases of the individual beam segments. The lenses create interference patterns that can be analyzed to determine the relative phase. Concentric circles represent lens contours.**

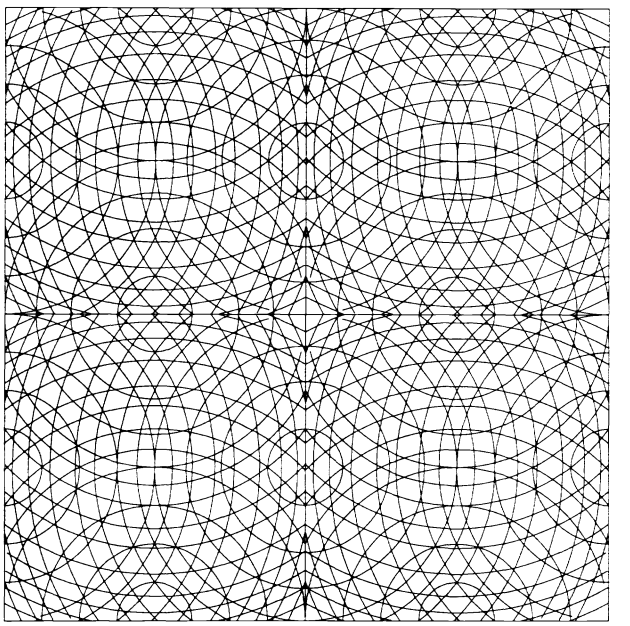

**Figure 3 - Matrix phase comparator. Each segment creates a focus on all four edges. Thus each segment can be compared to all the surrounding segments.**

## 2. ADAPTIVE OPTIC TESTBED

### 2.1 Brassboard

The basic elements of the brassboard are described in Figure 1. Light from a He-Ne laser is expanded in a six inch beam expander to form a single large coherent beam. This light is then segmented into a series of individual beams with a beam sampler, which consists of an array of small beam sampling mirrors. These mirrors are separated and misaligned so that they produce an array of beams with widely different tip and tilts. These individual beams are then steered onto a segmented adaptive optic. The current system uses the same 2x2 mirror elements that were described in reference 17, although plans for a 4x4 system using a mirror borrowed from the Air Force Phillips Lab, and an 8x8 system to be fabricated by a contractor are in process. Figure 1 shows the planned configuration for the 8x8 system. The current system is very similar, with the exception that only 2x2 elements are used and the tip/tilt sensor uses analog electronics directly coupled to the VME computer A/D converter. Most of the simulations in this paper are designed for the 4x4 mirror system, although extension to the full 8x8 system is straightforward.

Once the light leaves the adaptive optic, it is directed onto a series of different sensors by use of beam splitters. Three different sensors are typically used. The first element is a Shack-Hartmann wavefront sensor with each lenslet segment mapped to one segment of the mirror array. This sensor is used to measure the individual beam pointing and alignment, and to provide feedback control for mirror array pointing. The second sensor is a phase comparator that determines the relative piston phase of each segment. The third is a far-field sensor that is used to measure the overall performance of the system (Strehl or other beam quality measure).

Since this brassboard is designed to allow testing of evolutionary improvements, each of these sensors has a number of different embodiments. The 2x2 system uses an analog tip/tilt sensor with discrete lenses and UDT position sensitive detectors. It is extremely sensitive and provides high bandwidth control of mirror pointing. Each loop is closed individually at approximately 200 Hz bandwidth, although it would not be difficult to extend this since the actuators can be used up to 1000 Hz in a closed loop feedback system. An alternative embodiment of this sensor is scaleable to a large number of beams. In this case the sensor consists of a low pixel count CCD detector (typically 64x64) that can be read out at high speed (~2 kHz). We used a DALSA CA-D1-64 for these experiments. Light was directed onto the detector through a pupil remapped binary optic lenslet array that is described in more detail in a companion paper[22]. This element was designed for maximum image distance, while maintaining small spots for good separation. Hence pupil remapping was used to eliminate the need for re-imaging optics between the lenslet array and the detector. More

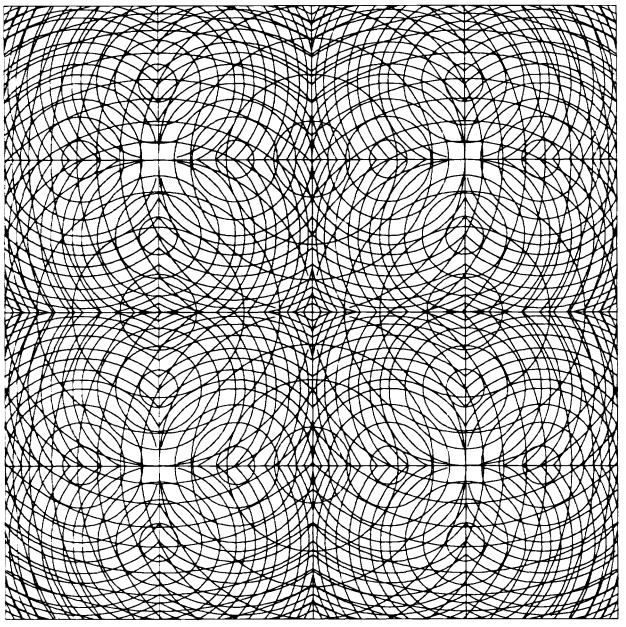

**Figure 4 - Hierarchical scaling to 4x4 segments. Each set of 2x2 segments is treated as a single element which are group phased using the same method. The focal spots fall in between the spots from the individual elements.**

information on this optic is presented in later sections and in other work[22].

The other primary sensor is the phase comparator system. This system uses specialized binary optics that are designed to compare the phase of individual beams two at a time. Figure 2 shows how, in a typical 2x2 section of the adaptive mirror, the phase is compared first for the top two beams, then the right two, the bottom two and the left two. In this way every segment is compared against all adjacent segments. This information is used to drive the mirrors to the position required for optimum phase. There is one element of redundancy (since phases are compared all the way around the 2x2 section) that can be used for noise reduction and error checking. This basic 2x2 phasing scheme is used for all the phase computations, with different arrangements used for different scaling systems.

Two alternative scaling methodologies are depicted in Figures 3 and 4. In Figure 3, each mirror segment is compared to mirror segments on all four sides. To compute the desired phase of the total system, a matrix algorithm must be solved at each iteration. The other method, depicted in Figure 4, is hierarchical. Hierarchical scaling has advantages for systems with many degrees of freedom[17,20,23]. Each 2x2 section is treated as a single segment of a larger (super-segment) that are themselves part of a 2x2 super section. These 2x2 super beams are

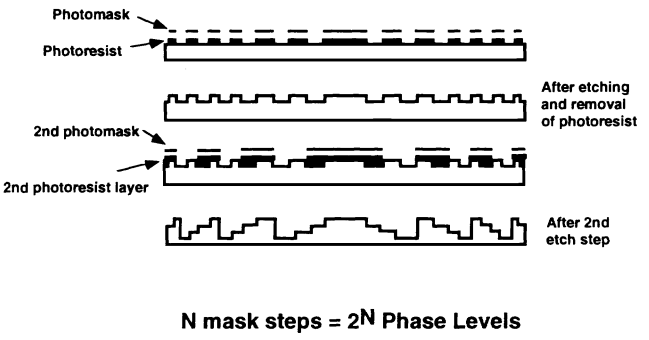


**Figure 5 - Fabrication sequence for binary optic with four phase levels**

themselves grouped together to make up even larger elements (4x4) and so on in a hierarchical fashion, until all the segments have been phased. This method reduces the number of phasing operations which must be performed. For an 8x8 system, there are 16 2x2 groups with four comparisons each, 4 4x4 groups (with four comparisons) and one overall 8x8 group with four comparisons. Thus 16·4 + 4·4 +4= 84 phase comparisons must be performed. This is in comparison to 64·4 - 2·8 - 2·7 = 226 comparisons which need to be performed with the matrix method. As the number of segments grows larger, this scaling becomes even more dramatic. It should be noted that shear systems[16] which compare the phase of adjacent segments are similar to the matrix comparison case, since every element is compared to all its neighbors.

The actual phase relationship between any two adjacent beam segments is determined by the interference pattern created by the focused beams. When the tip/tilt of the adjacent beams is adjusted to be fairly similar, then both the matrix and the hierarchical phase comparators will create overlapping spots. If these beams are in phase, they will constructively interfere. However, an out-of-phase condition will be indicated by an interference pattern. This pattern can be analyzed to determine the relative phase between the adjacent segments. A description of this procedure is given in section 2.5.1.

We fabricated specialized binary optics to perform both types of phase comparison, matrix and hierarchical, and these optics are described in section 2.2.

## 2.2 Binary optic descriptions

Binary (or diffractive) optics are fabricated using similar processes to those employed in integrated circuit manufacture. The desired optic is designed as a series of masks, which together can be used to produce an arbitrary surface profile. These masks are laid out using a series of

optical design tools and IC mask layout software. They are then transferred to a chrome mask set that can be used to contact print onto the desired substrate using photo-lithography. The profile is built up by reactive-ion etching the pattern into the substrate, and then repeating the procedure with a different mask and depth. Figure 5 shows an example of a Fresnel lens that is fabricated using this technique using only two photo-lithography and etch cycles. We have typically used 4 cycles, thereby building optical structures with 16 levels, which are nearly diffraction limited in performance and have >99% efficiency.

One of the primary purposes of this testbed is to develop techniques to simplify the set up and optics of adaptive optics. Our primary strategy is to use binary optics where appropriate to reduce the complexity of the optical system, placing complexity in the design of the binary optic, instead of in the overall optical system. This is accomplished by using binary optics for both the tip/tilt sensor and the phase comparator. The binary optics were designed assuming a full 8x8 system would be constructed, although, depending upon the actual adaptive optic in use, it may be that only a portion is actually used at one time.

### 2.2.1 Tip/Tilt Sensor Binary Optic

The tip/tilt sensor is essentially a regular lenslet array that images onto a CCD detector. While an existing lenslet array could have been used to construct this sensor, it would not have been optimized for this application, and would have required the use of re-imaging optics between the array and the detector. Instead we designed and fabricated a custom binary optic that matched the desired characteristics of both the adaptive optic and the detector array. As depicted in Figure 1, light from the adaptive optic is demagnified onto the lenslet array. The light is split into an 8x8 array of lenslets that are focused onto the detector array. Since the spot size from each of these lenslets is $2\,f\#\,\lambda$, and an 8x8 arrangement of spots is desired, each spot has an approximately 8x8 pixel region. To avoid spot overlap and other problems, the actual spot size must be considerably less than this (2x2 or 3x3 pixels). This leads to a fairly small $f\#$ ($f/d$) requirement ($f\#$ = 37.5 for 16 μm pixels). If $d$ is assumed to be the same size as the 8x8 pixel block, then the focal length of the lenslet array is very short (5 mm in this case). This leads to a fairly insensitive wavefront sensor since the sensitivity depends upon the focal length of the lenslets ($f$). However, because of the arbitrary nature of the binary optic surface, there is no reason to assume that the lenslet array must be the same as the detector array. Thus the same $f\#$ can be achieved with a much longer focal length. The lenslet array then consists of an optic that is $M$ times bigger than the detector array (4 for our initial design). It should be pointed out that the same thing can be accomplished by using re-imaging optics between the lenslet array and the detector. However, it is no more difficult to fabricate a remapped lenslet array than the direct one, and the overall optical system is much simpler with fewer potential aberrations. More information on this optic is presented in reference 22.

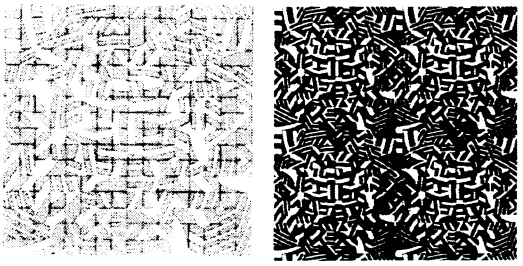

(a) (b)

**Figure 6 - Matrix phase comparator mask layout for (a) single segment and (b) four segments.**

### 2.2.2 Phase comparators

One of the unique advantages of binary optics is that totally arbitrary surfaces can be constructed. For example, lenses can be constructed in arrays with 100% fill factor and aspherical shapes can be used. The tip/tilt sensor demonstrates that these lens segments need not even be on-axis. This arbitrary nature can be used to build more sophisticated optics so that several different operations can be performed by specified apertures. This is accomplished as follows: the overall aperture is broken up into a series of small rectangular or square facets (maybe only a few micrometers in diameter). Each facet is assigned a particular function; however, adjacent facets are not required to have the same function. Figure 6 shows an example of this for a small portion of the aperture. In this case every other facet within a segment focuses on an alternate edge of the segment. Since there are a large number of facets within each segment, the effect is of an overall sampling of the whole segment. Since these facets add coherently at the focal plane, if there are a sufficient number and they are arranged correctly, the desired far-field pattern may be obtained. Thus the overlapped optical systems described in section 2.1 can be constructed in this fashion. This technique is called aperture multiplexing[20] because the same aperture can be used to perform multiple shared functions by spatially switched operations. Other examples of this have been previously reported[20].

Figure 6(a) and (b) show how this technique is applied to construct a matrix phase comparator. Each segment is broken up into facets that focus light alternately on all four edges. All segments are the same, and, since every segment shares four edges with its neighbors, the desired matrix

pattern is created where light from adjacent segments can be compared. Diffraction from faceted apertures can lead to spurious intensity patterns and so careful modeling and design is necessary. This issue has been addressed in reference 24.

The hierarchical phase comparator is constructed in a similar manner, except that some of the facets from each segment are devoted not to the comparison of light with an adjacent segment, but to comparison with other levels in the hierarchy. Since each successive level has four times as many segments as the previous one, the number of facets is adjusted to give relatively uniform intensity. Figure 7 depicts the mask layout. Comparisons between model and experimental data can be found in reference 24.

One problem with this method of constructing the hierarchical structure is that the spot size for each successive tier is half that of the last (because the effective aperture size is twice as big). This requires scaling the phase comparison algorithm accordingly.

It turns out that a hierarchical system may also be constructed using the matrix binary optic, although used in a slightly different fashion. In a hierarchical system, each of the 16 2x2 elements are phase compared to bring them in phase. Since each of the elements is in phase with respect to the others, it isn't necessary to extract phase information for the next tier in the hierarchy from all of the segments. Only one segment is really needed. Thus by choosing to phase only certain sets of segments, the hierarchical result can be obtained using the matrix phase comparator. For the 8x8 system, only 84 spots are used instead of the 226 that are generated. In later sections it will be shown that this phasing can be performed all at once. It isn't necessary for each 2x2 group to be phased first. This also has the advantage that all the spots are the same size, obviating the need for scaling the phasing algorithms.

### 2.3 Simulation testbed

A simulation testbed was created in order to develop and evaluate binary optic interpretation algorithms and to enable simulation of feedback control for the segmented adaptive optic. The structure of the simulation testbed is similar to that of the brassboard hardware (Figure 1). The simulation extends the brassboard concept to a 4x4 adaptive optic configuration. Each of the sensing functions (phase, alignment, beam quality) is implemented by passing the wavefront coming off the adaptive optic segmented mirror through a binary optic and focusing it onto a 128x128 pixel CCD camera. These functions are replaced in simulation by their Fourier transform equivalents.

The adaptive optic dynamic simulation produces true values for the tip, tilt, and piston of each mirror segment. These

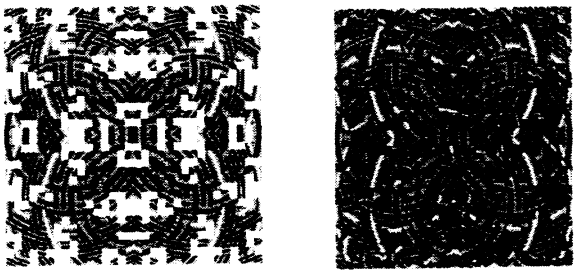

(a) (b)

**Figure 7 - Mask layout for a portion of the hierarchical phase comparator. (a) Missing facets are reserved for higher tiers, (b) all tiers included.**

are fed in turn to the three binary optic simulations. These simulations emulate the CCD camera images produced by the appropriate binary optic: the array phase comparator image, the Hartmann sensor (or tip/tilt sensing algorithm), and the combined beam.

Next, the phase, alignment, and Strehl algorithms compute relative phase between beams, tip and tilt for each beam, and the Strehl ratio for the combined beam.

The function of the feedback control system is that of a regulator: to keep each laser beam bouncing off a segment of the adaptive optic aligned and in phase with all of the others.

### 2.4 Binary Optic Simulations

The binary optic sensors were designed with the assistance of a detailed simulation that[24] solved analytically for the contribution of each segment of the diffractive optics wavefront sensor. This simulation proved to be too time consuming to be practical for control systems simulation.

A simplified model of the binary optic (which we have called the combined model) was developed for the control system modeling. These simplified simulations take as inputs the tip, tilt, and phase information for each segment of the adaptive optic and produce CCD camera monitor images. The estimation functions described in section 2.5 process the camera images and report the appropriate outputs (phase, tip, tilt, or Strehl ratio).

The simulation of each of the binary optic sensors is governed by a data matrix which specifies the location of each focal point on the CCD camera image and indicates which segments of the adaptive optic have portions of their beams directed onto these foci. Scaling factors are also specified to achieve the appropriate relative brightness of each sub-image.

The tip, tilt, and phase inputs to these routines define a wavefront for each segment of the adaptive optic. The

geometry of the optical system is such that the Fourier transform of the wavefront in the adaptive optic plane is an adequate representation of the wavefront in the image plane. The simulation routine consists of computing the Fourier transform of each wavefront to obtain the field distribution in the image plane and constructing the entire field distribution through coherent addition. Taking the absolute values of the field distribution yields a close approximation to the image produced on a CCD camera in a lab setting. More detail on these simulations is presented in another paper[24].

### 2.5 Estimation functions

Analytical estimation functions extract phase, tip, tilt, and beam quality information from the CCD camera images.

#### 2.5.1 Two beam relative phase estimation

The basic two beam relative phase estimator forms the basis for estimating phase relationships within an array of any size. For this work, each segment of the adaptive optic is assumed to be rectangular. A dead space between mirror segments is also accommodated by the algorithm.

Phase estimation was obtained through an analytical solution. Figure 8 illustrates the combination of two rectangular wavefronts. The corresponding adaptive optic segments lie parallel to the X-Y plane, but may be offset in the Z dimension from each other. This offset in Z, as well as any pre-existing path-length differences between the incident beams, causes a phase difference between the two light beams that must be eliminated for coherent beam combination. Light from the adaptive optic segments is focused through a lens onto a CCD camera at a distance f from the x-y plane along the Z dimension. The height of the mirrors is $D$, and they are separated by a distance $\delta$.

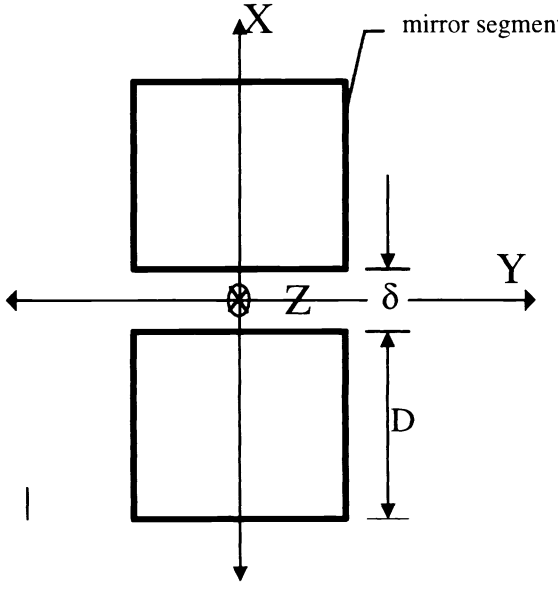


**Figure 8 - Geometry for two beam phase estimation. Two mirrors in the X-Y plane have height D and are separated by a distance δ.**

Figure 9 shows the image plane patterns from several different phase differences. These may be summed across $y$ to create a function of $x$, $\Sigma\, I(x)$, as shown in the lower portion of the images. This summing results in a more robust computation of the phase, since the averaging serves to reduce error terms such as CCD camera noise. An analytical expression for $\Sigma\, I(x)$ may be written:

$$\sum I(x) = \theta + \frac{k}{2} \cdot \mathrm{sinc}^2\left(\frac{D \cdot x}{\lambda \cdot f}\right) \cdot \left[ 1 + \cos\left(\frac{2 \cdot \pi \cdot x}{\lambda \cdot f} \cdot (D+\delta)\right) \cdot \cos(\phi) + \sin\left(\frac{2 \cdot \pi \cdot x}{\lambda \cdot f} \cdot (D+\delta)\right) \cdot \sin(\phi) \right] \quad (1)$$

)

where θ is a constant offset term, k is a scaling factor, f is the focal length, and φ is the phase difference between the two mirrors. This may be solved using a simple least squares fit algorithm to obtain k, k*cos(Φ), and k*sin(Φ), and θ.

A very simple phase algorithm was used for initial tests in the lab. The inspiration for this scheme was the observation that the summed values of Figure 9 have three lobes, and, when the beams are in phase, the sizes of the two outer lobes are equal. An indication of the phase error is constructed by computing the areas of the two outer lobes and taking their difference. If only one of the outer lobes is discernible, a fixed error in the appropriate direction is indicated. This algorithm proved serviceable in initial tests; laboratory results are shown in Figure 12. It was abandoned in favor of the analytical solution (above) in order to obtain more accurate and linear phase estimations.

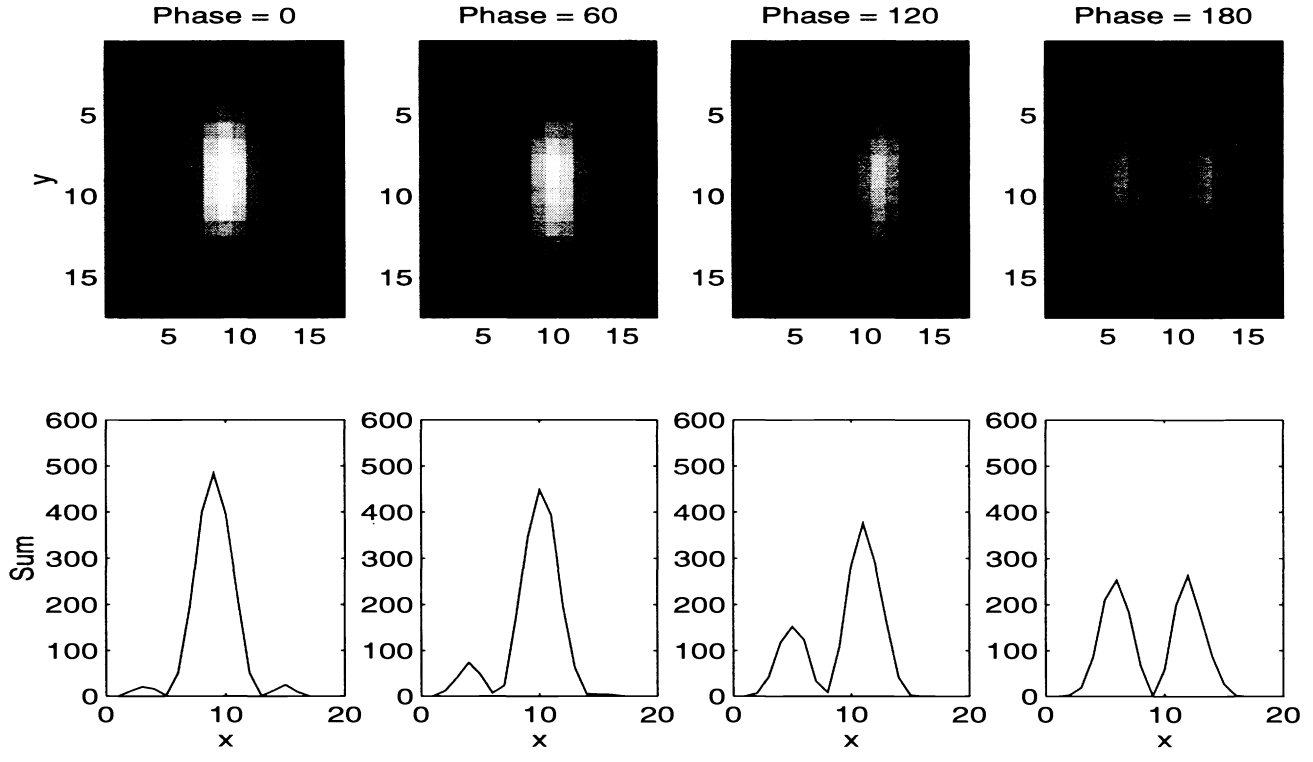


**Figure 9 - Ideal two beam phase estimation data. Computed phase is accurate to 6 decimal places.**

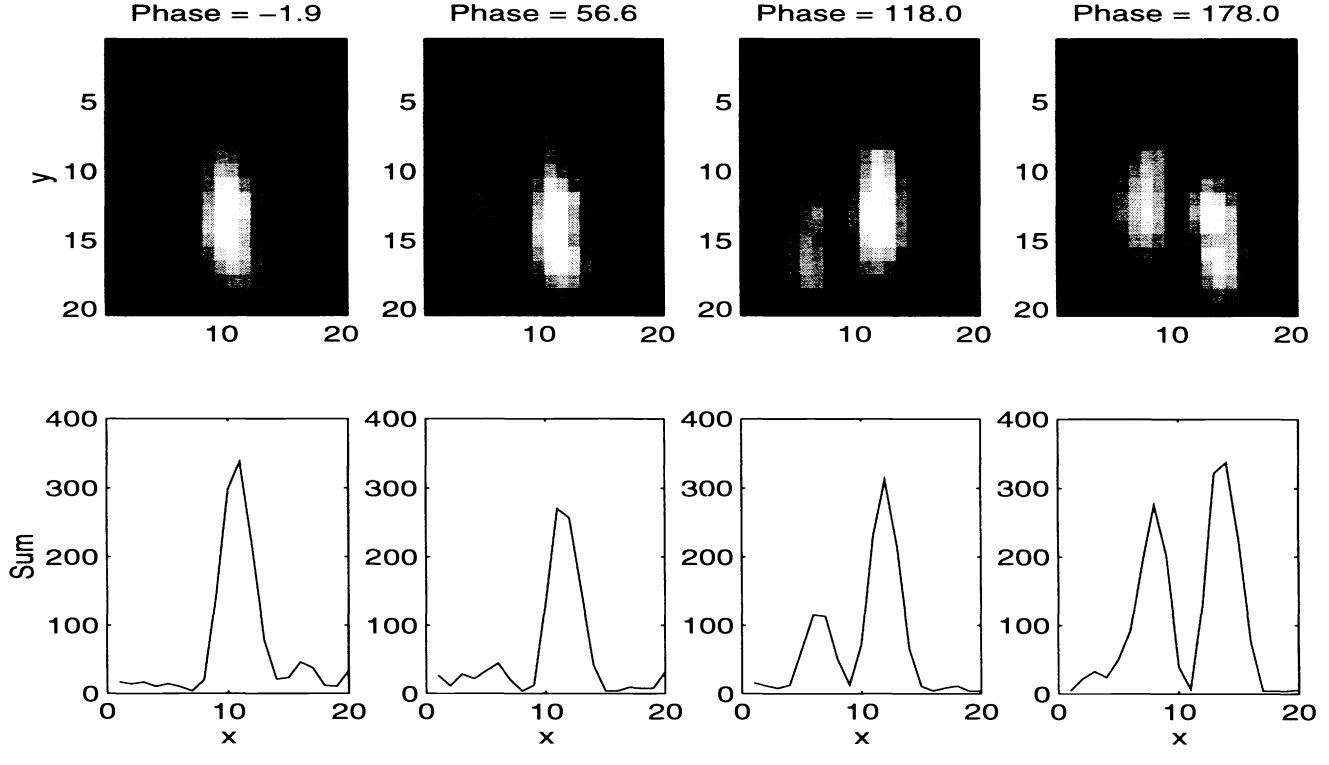


**Figure 10 - Actual two beam phase estimation data. Computed phase is shown for each image. Rows containing saturated entries are thrown out for each image.**

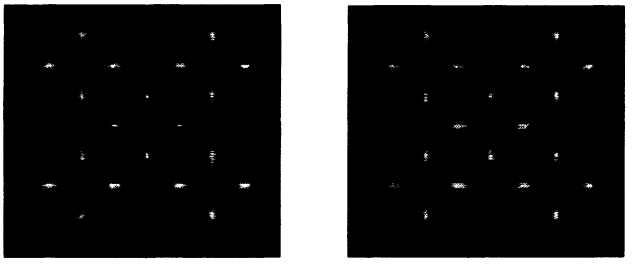

(a) (b)

**Figure 11 - (a) Hierarchical and (b) modified hierarchical phase comparator images for zero phase condition.**

### 2.5.2 Array phase estimation

Hierarchical control algorithms were implemented for both the matrix phase comparator binary optic and the hierarchical phase comparator binary optic. Each is based on the two beam phase estimation of 2.5.1.

The lowest tier of our hierarchical comparator consists of 4 adaptive optic segments arranged in a 2 by 2 configuration. In the upper left hand quadrant, four larger spots compare the phases of each beam to its two neighbors through the use of the two beam phase estimator. Each spot is a far-field diffraction pattern resulting from the combination of beams from two adjacent adaptive optic segments. Since there are three independent unknowns (three relative phases) and four results of four phase comparisons, one redundant measure is available for sensibility checking or averaging. The same lowest-tier phase computation takes place for each of the quadrants.

In the center of the images, there are four smaller spots which each result from combining eight beams total, i.e. all four beams from each of two quadrants. The phase information estimated from these sub-images is invalid unless the beams of the lowest tier are aligned. In using the two-beam comparison algorithm of Equation 1 for this computation, the separation $\delta$ is assumed to be negligible. For our brassboard system, this is a valid assumption.

The result of the 4x4 array phase estimator model with the tip, tilt, and phase inputs all zero was

$$\begin{bmatrix} 0 & -0.3326 & 3.2440 & 3.7855 \\ 0.5436 & -0.1089 & 2.9488 & 3.4904 \\ 3.2705 & 3.2302 & 6.5145 & 6.1806 \\ 2.7716 & 2.7313 & 6.4197 & 6.4056 \end{bmatrix}.$$

Each element of the matrix specifies the relative phase (in degrees, where 360 degrees equals 1 wavelength) of the corresponding mirror with respect to the upper left hand mirror. These estimations are non-zero due to interference among the individual far-field images. This matrix therefore defines a null offset condition to which the phase must be servoed to obtain true zero phase.

This approach may be extended to an 8x8 array of mirrors by scaling the phase sensor appropriately. This approach suffers from two disadvantages: (1) Each successive layer of the hierarchy causes a smaller spot to be generated, thus increasing computation error as the system is scaled up; and (2) the entire array must be phased up in steps, from the lowest level of the hierarchy to the highest. (In practice, we do not impose these steps on the processing. They were imposed by the nature of the algorithms, in which the higher level estimations were not correct until the lower levels were phased up). Because all the phasing operations are performed in parallel, the hierarchical structure performs the wavefront reconstruction automatically. Therefore no separate reconstruction step is necessary.

To obviate both of these problems, a modified hierarchical phase sensor was simulated. It is based on the matrix phase comparator. Operation is just as described above, but with higher level comparisons based on the comparison of one single mirror from each of the two lower level hierarchies. All spot sizes are thus equal, and all beams in the array may be brought into phase after a single estimation of the entire array state in those conditions where the tip and tilt of the beams are already aligned.

### 2.5.3 Alignment sensor

The left hand column of Figure 15 contains images created by the simulated alignment sensor. The 4x4 tip and tilt sensor image is divided conceptually into 16 boxes. Each box holds a spot thrown by the appropriate segment of the adaptive optic. After power-up, a calibration routine must be run during which each spot is pointed into its alignment box, and the correct location for the centroid of that spot on the CCD camera image is determined. During feedback control of the adaptive optic, the alignment sensor algorithm simply determines the centroids for each box, subtracts off the desired centroid, and converts this error to a tip or tilt according to the system geometry.

### 2.5.4 Strehl sensor

We desired an indicator of total combined beam quality to measure our success. The simulated sensor was simple: a composite beam was constructed and focused onto a single spot. The peak value of the camera image is divided by the ideal peak value to form the Strehl ratio.

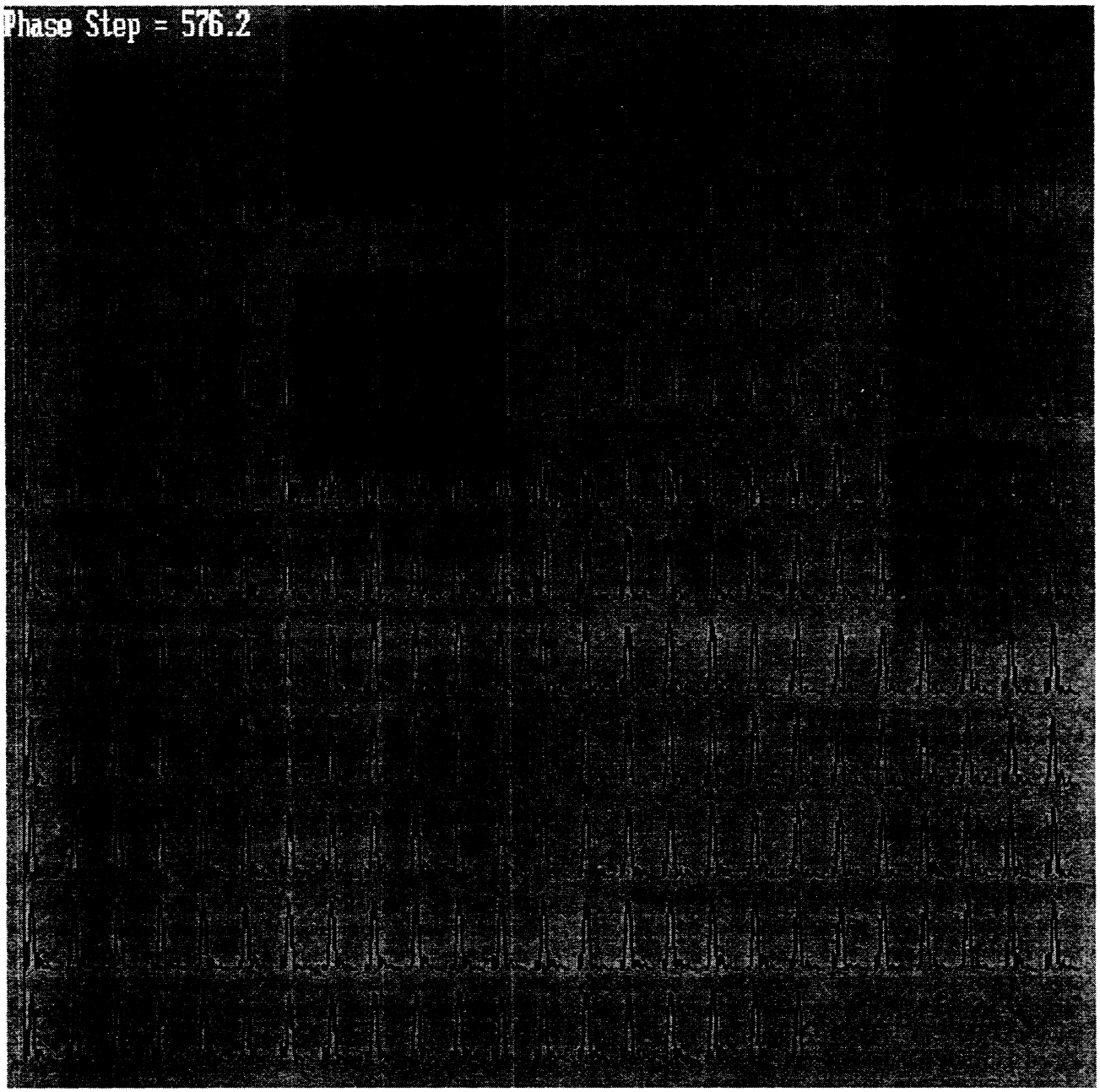


**Figure 12 - Laboratory data of two beam combining using primitive phase estimation algorithm. Each row of image contains image sums for 1 second of data at 25 Hz. Optical table was struck on 4th row, 11th image. System recovered by 6th row, 1st image.**

## 3. EXPERIMENTS

### 3.1 Brassboard experiments

The 2 by 2 brassboard system was tested using conventional Hartmann sensors for tip and tilt determination. Both of the two-beam phase estimators described in section 2.5.1 were implemented. The laboratory data illustrated in Figure 12 was collected using the primitive original phase algorithm. The figure shows phase sums for two-beam combination. Images were collected and summed at 25 Hz. In this sequence, the control loop maintained a near-zero phase until the optical table was struck. The signature temporarily disappears while tip and tilt are restored. Phase is perturbed for about 1.7 seconds as the table continues to shake.

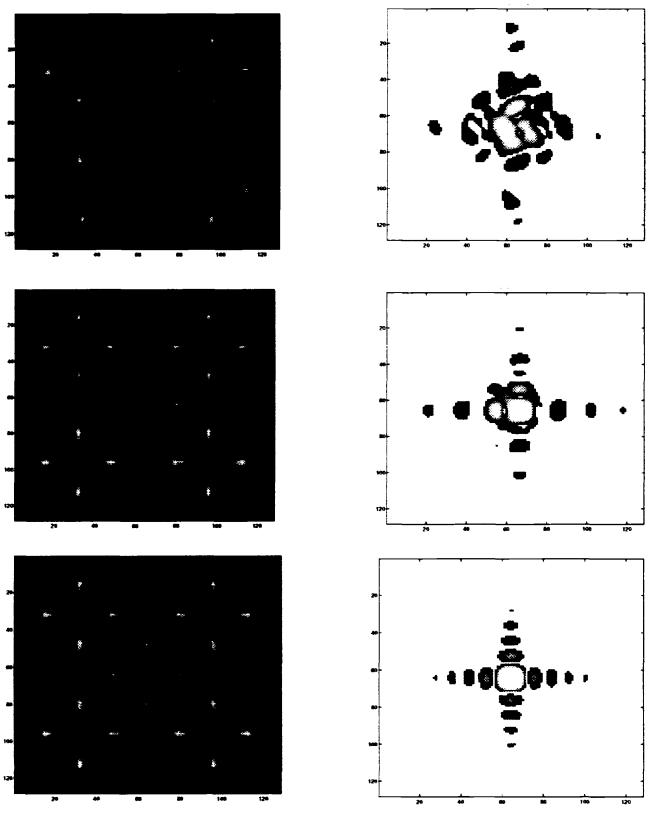

**Figure 14 - Simulation of section 3.2.1. Phasing only with hierarchical array comparator.**

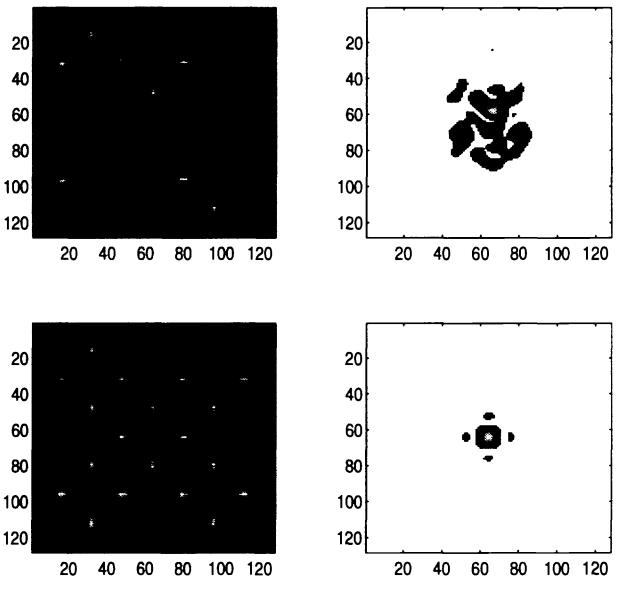


**Figure 13 - Simulation of section 3.2.2. Phasing only with modified hierarchical array sensor.**

## 3.2 Simulation experiments

### 3.2.1 Phasing only with hierarchical phase comparator

Our first experiment phased up the mirrors of the adaptive optic from a random phase condition and with tips and tilts perfectly aligned. We servoed to the phase null-offset mentioned in section 2.5.2 using the hierarchical phase comparator of Figure 11. Figure 14 shows the progression from a random phase condition to the aligned state. Each row shows the image from the phase comparator (left) and the Strehl sensor (right) at a processing iteration. The background color on the Strehl sensor has been changed from black to white for improved clarity. In iteration 1, we see the phase initialized to an arbitrary condition. The Strehl sensor indicates a Strehl ratio of 0.29. In the next iteration, the lowest tiers of the hierarchy have been phased up, but they are not in phase with each other. The Strehl ratio is 0.76. One more iteration is required to bring the mirrors into phase for a Strehl ratio of 1.

For the hierarchical phase comparator the higher tier focal spots are composed of light that is collected from a group of the lowest tier. Thus initially, when all the segments are unphased, the Strehl ratio of these higher tier focal spots is low. The phasing algorithm therefore doesn't work very well, and little phasing is achieved among the higher tiers until all the lower tiers are phased. For a two tier system it takes an iteration to phase the lower tiers and then an additional iteration to phase the higher tiers.

### 3.2.2 Phasing only with modified hierarchical phase comparator

As an alternative arrangement, the modified phase comparator of Figure 11b was tested. In this arrangement only one segment from each of the higher tiers is sampled by the binary optic. The spot size is the same as the lower tiers since each tier now samples the same size region. Furthermore, the Strehl of individual spots is not degraded because only individual segments are sampled. With this technique the phase sensor now has sufficient information in a single frame to infer the phase of the entire mirror array.

Operation of the modified phase comparator (Figure 11b) is shown in Figure 13. Only a single array phase estimation is required to bring the Strehl ratio to 0.997 in simulation.

In practice, it is likely that either method would work equally well, since once closed loop operation was established, the control system would keep the mirror array in good phase most of the time, tolerating only relatively small errors. This would keep the Strehl of higher tier focal spots high enough so that the phasing algorithm has a chance to work.

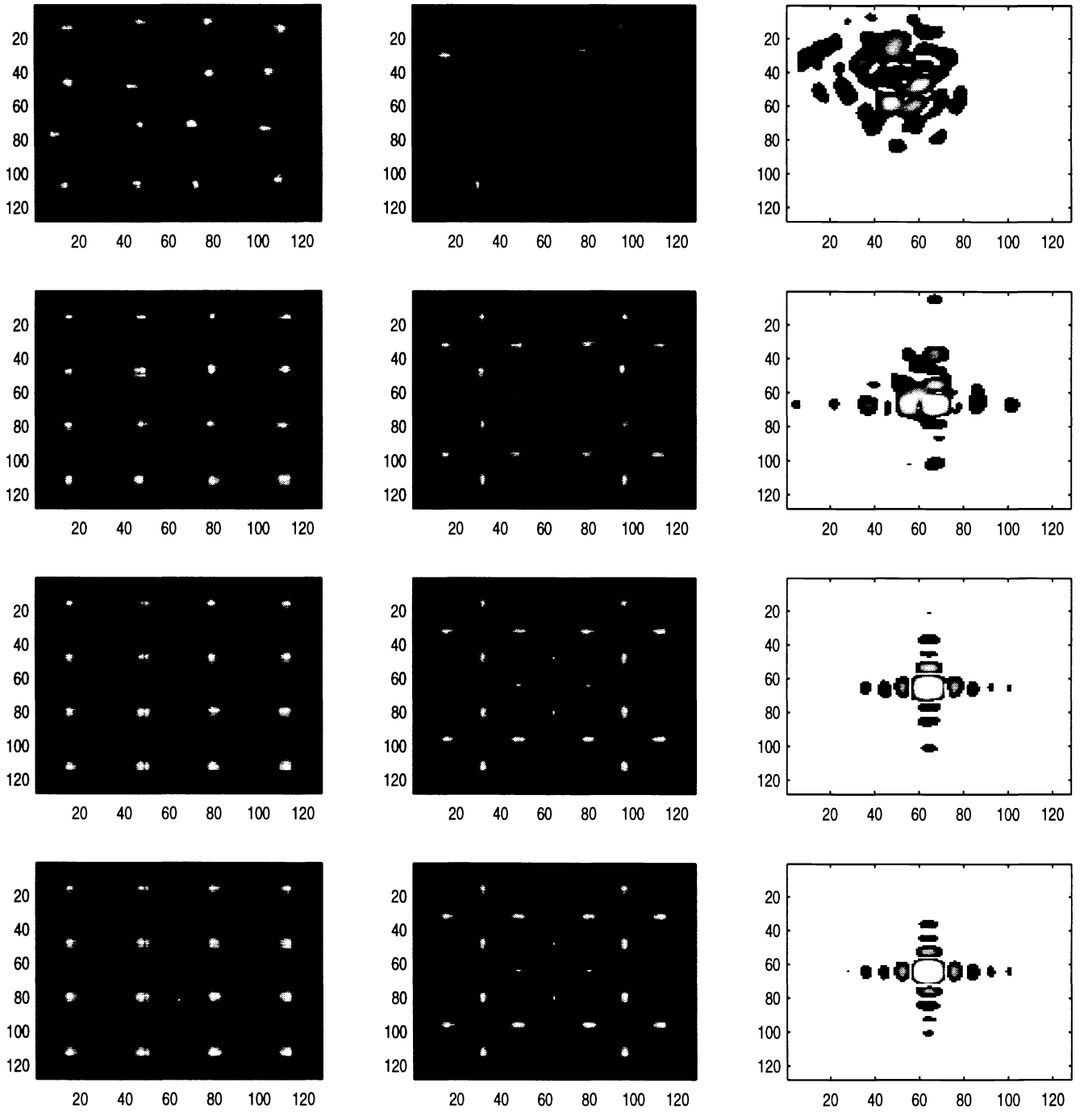


**Figure 15 - Simulation experiment of section 3.2.2. Concurrent phasing and alignment requires only one iteration more than phase only experiment.**

### 3.2.3 Concurrent phasing and alignment

So far, phase alone was considered as a part of the overall system, and the tip/tilt of each beam was considered to be perfect. In practice, however, the tip/tilt is also controlled by a Hartmann sensor (perhaps at higher bandwidth). Since a misalignment in tip/tilt can lead to spot position changes in the phase sensor, there is the possibility of a strong coupling between the tip/tilt loop and the phasing loop.

Figure 15 shows simultaneous operation of the phasing and tip/tilt algorithms. The left hand column shows the tip and tilt of the mirror segments initialized at random, as are the

mirror phases. In a single step, the tip and tilt states are substantially rectified, as are the phases of the lowest level of the phase hierarchy. A second processing step rectifies the lowest level phase discrepancies. One additional cycle is required to bring the Strehl ratio up to 0.98.

This example illustrates an important fact underpinning this work: the diffraction patterns from which phase is estimated are relatively insensitive to disturbances in the tip and the tilt of the mirror segments. This can be seen in the individual images: as the tip/tilt of a beam is varied, the overlap from adjacent segments changes, However, the interference between the two remains only a function of the relative piston phase. Thus, even though the focal spots are degraded, the basic piston information is still present, and the phasing algorithm has no trouble distinguishing it.

## 4. Conclusions

We have demonstrated operation of all the basic components of a closed loop system for tip/tilt and piston control of segmented adaptive optics. We used binary optics technology to implement a series of custom optical sensors for directly measuring the tip/tilt and piston phase of the mirror segments. We have simulated a number of hierarchical scaling algorithms and have shown that excellent system performance is obtainable. The system relies on two-at-a-time comparison of phases across the system aperture that operate well even in the presence of significant noise.

While all the simulations are essentially complete, further integration into the testbed is needed. Two different binary optics have been fabricated and tested optically, but they have not been fully integrated into the system. We have tested all the basic elements: operation of the binary optics, ability to phase two beams using a binary optics phase comparator, the noise performance of the phasing algorithms, and closed loop performance of the tip/tilt and phasing systems. Full implementation on the existing 4x4 deformable mirror system is the subject of our continuing research.

## 5. References


[1] R. D. Neal, T. S. McKechnie and D. R. Neal, "System requirements for laser power beaming to geosynchronous satellites, SPIE 2121 Laser Power Beaming, pp. 211-221 (1994).

[2] R. Miles, G. Brown, W. Lempert, D. Natelson, R. Yetter, J. Guest, G. Williams, and S. Bogdonoff, "Radiatively driven hypersonic wind tunnel," AIAA-94-2472, 18th AIAA Aerospace Ground Testing Conf., Colo Springs., CO., June 20-23, 1994.

[3] J. R. Felty, "DOE reactor-pumped laser program," SPIE Vol. 2121, pp. 2-9 (1994).

[4] D. K Monroe, "Space debris removal using high-power ground-based laser," SPIE 2121, pp. 276-283 (1994).

[5] Long range imaging

[6] J. P. Bell, D. R. Pnikvar, "THUNDERBALL: a power-beaming architecture for missile defense," SPIE Vol 2121, pp. 284-293 (1994).

[7] J. F. Figueira, "Development of KrF lasers for fusion," Proc. of Intl Conf. on Lasers '89, pp. 58-62, STS Press, McLean, VA (1990).

[8] V. N. Litvinenko, J. M.J. Madey, N. A. Vinokurov, "Component technologies for a recirculating linac free-electron laser," SPIE Vol. 2121, pp. 21-37 (1994).

[9] N. Griff, D. Kline, S. Lissit, "Space based lasers for strategic defense," Proc. of Intl Conf. on Lasers '89, pp. 180-188, STS Press, McLean, VA (1990).

[10] H. Lurie et al, "Alpha high-power chemical laser program," SPIE Vol. 1871-14 (1993).

[11] R. L. Gullickson, "Advances in directed energy technology for strategic defense," Proc. of Intl Conf. on Lasers '89, pp. 270-277, STS Press, McLean, VA (1990).

[12] W. P. Latham, "A review of laser device coupling techniques," SPIE 1224, pp. 184-201 (1990).

[13] M. J. LeFebvre, E. L. Cuellar, G. L. Taylor, S. M. Stahl, T. K. Barrett, and D. G. Sandler, "Point ahead compensated illuminations tests using the 500-channel innovative science and technology experimental facility adaptive optics system," SPIE Vol 2201, pp. 373-380 (1994).

[14] P. D. MacNeal, K. A. Jewett, "Design and fabrication of a large primary reflector structure for space laser power beaming," SPIE Vol. 2121, pp. 91-98 (1994).

[15] G. A. Hebner, "Reactor-pumped laser experimental results," SPIE Vol. 2121, pp. 10-20 (1994).

[16] D. G. Sandler, L. Cuellar, M. Lefebvre, T. K Barrett, R. Arnold, and S. Stahl, "Recent results for visible Rayleigh guide star atmospheric experiments," SPIE 1920, pp. 42-51 (1993).

[17] "Multiple Laser Beam Combining and Phasing Using Closed-Loop Control," D. R. Neal, T. G. Smith, G. R. Eisler, J. L. Wilcoxen, R. R. Rosenthal, SPIE 1920, pp. 9-19 (1993).

[18] D. S. Action, R. B. Dunn, "Solar imaging at the National Solar Observatory using a segmented adaptive optics system," SPIE 1920, pp. 348-352 (1993)

[19] P. L Wisinowich, M Lloyd-Hart, B. A. McLeod, D. Colucci, R. G. Dekany, D. Wittman, J. R. Angel, D. W. McCarthy, Jr., W. G. Hulburd, D. G. Sandler, "Neural network adaptive optics for the multiple-mirror telescope," SPIE 1542, pp. 148-158 (1991).

[20] D. R. Neal, M. E. Warren, J. K Gruetzner, T. G. Smith, R. R. Rosenthal, T. S. McKechnie, "Mulitiered wavefront

sensor using binary optics," SPIE Vol. 2201, pp. 574-585 (1994).
[21] R. K. Tyson, "Measuring phase errors of an array of segmented mirrors with a single far-field intensity distribution," SPIE 1542, pp. 62-75 (1991)
[22] D. R. Neal, J. D. Mansell, J. K. Gruetzner, M. E. Warren, R. Morgan, "Specialized wavefront sensors for adaptive optics," SPIE 2534-32 (July 1995).
[23] A. Lazzarini, G. Ames, "Methods of hierarchical control for a segmented active mirror," SPIE 2121, pp. 147-158 (1994).
[24] J. K. Gruetzner, S. D. Tucker, D. R. Neal, and K. Simmons-Potter, "Optical and control modeling for adaptive beam-combining experiments", SPIE 2534-11 (July 1995).